REALISTIC SIMULATION OF INSTANTANEOUS NEARSHORE WATER LEVELS DURING TYPHOONS

Fabien Rétif [1], Frédéric Bouchette [1], Patrick Marsaleix [2], Jiing-Yih Liou [3], Samuel Meulé [4], Héloïse Michaud [5], Li-Ching Lin [3], Kao-Shu Hwang [3], Nans Bujan [3], Hwung-Hweng Hwung [3], SIROCCO Team [2]

3D hydrodynamic simulations were performed on an area extending 600 km off Taiwan island for the period running from September 2011 to December 2012. We covered a winter Monsoon season and a summer season with 17 typhoons recorded. By comparing simulations and measurements during the TALIM typhoon, our model reproduces correctly the storm surge observed along the Wan-Tzu-Liao sand barrier (South-West Taiwan). By a modelling approach, we analyzed the regional hydrodynamic mechanisms which control the sea surface elevation at the Chung-Chin harbour. Tide is the dominant forcing of the water level with more than 1 meter above the mean sea level. Global currents contribute up to 80 cm to the water level but during the SAOLA typhon, the elevation reached 1 meter. The contribution of atmospheric forcings is lower but it can generate 30 cm of elevation (e.g. during GUCHOL and TALIM typhoons).

Keywords: instantaneous water level; wind; wave; current; typhoon; extreme phenomena

INTRODUCTION

The nearshore water levels vary at different timescales from minutes to years and are governed by the astronomical tides, meteorological conditions (pressure, wind), geostrophic currents, waves, local bathymetry and a set of others local and remote factors (Chelton and Enfield, 1986).

It often occurs that coastal regions experience high water levels during extreme events like typhoons. During this kind of events, it has been observed that the water level rises to several meters above its usual mean value, causing considerable damages to natural and artificial structures. The impact of extreme water levels along the coasts significantly increases while the mean sea level and the number of extreme meteorological events arise. To better understand and predict such an impact, it is fundamental to better characterize the conditions driving high water levels. This question has been studied by many authors during the 50 past years especially by a combination of measurement and simulations, which become more and more powerful.

Pugh (1987) emphased the effect tides and atmospheric conditions in storm surge. Wang and Elliott (1978) show the importance to include large scale forcings (open ocean conditions, local wind and non-local forcings) in nearshore modelling. Bowen et al. (1968) demonstrated that the wave setup is a key parameter to controlling negative and positive changes in mean water level at the shoreline. Dean and Bender (2006) or also Weber et al. (2009) highlighted that during storms, the wave setup can be the dominant process.

Dealing with most of the oceanographical forcings to the exception of waves (atmospheric conditions, global scale circulation and rivers), we propose to analyze the best forcings that control the water elevation along a sandy system located South-Western Taiwan during a contrasted range of meteo-marine conditions (complex bathymetries, warm currents and extreme meteorological events).

SETTINGS

The island of Taiwan displays a total of 1394 km of coastline, rocky shores to the East, flat and sandy beaches to the West (Doong et al., 2011).

Regional morphology

The West coast looks out onto the Taiwan Strait (TS)(Figure 1A), bounded by the China continent to the West and Taiwan to the East. It is a shallow strait 180km wide, 350km long and 80m depth in average. To the North, the strait is connected to the East China Sea (ECS), which is essentially a broad continental shelf extending hundreds of kilometers offshore ; and conversely the South is open to the South China Sea (SCS), where the shelf gradually narrows (Chiou et al., 2010). Waters in the South and East China Seas are exchanged through the strait.

[1] Montpellier II University
[2] Toulouse University
[3] National Cheng Kung University
[4] Aix-Marseille University
[5] SHOM

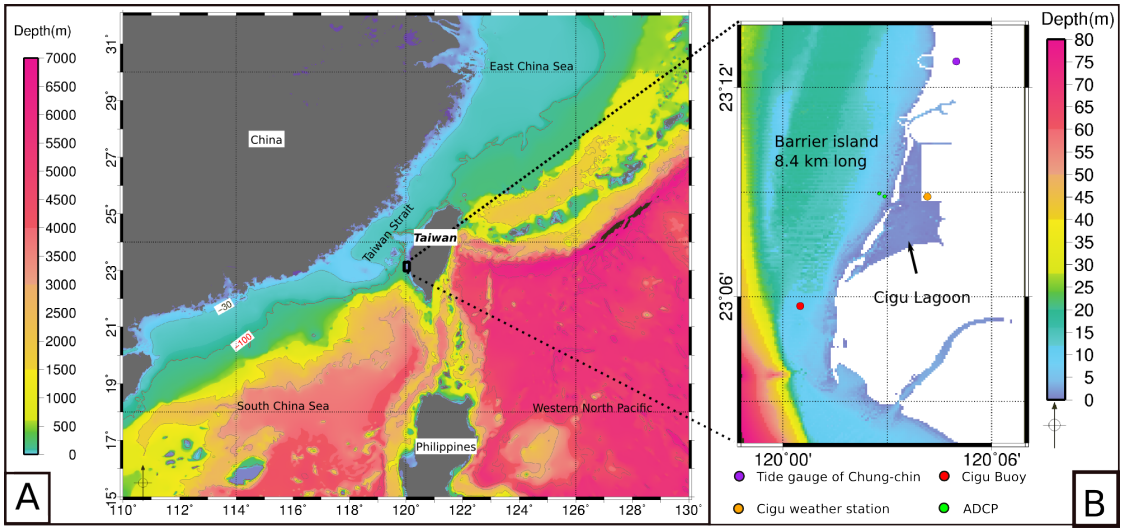

Figure 1: A) Bathymetry of the Taiwan strait; B) Bathymetry of the Wan-Tzu-Liao barrier and the location of the instruments.

Hydrodynamics

The astronomical tides in the TS are primarily semidiurnal and has a large spatial variation (Zhang et al., 2010) due to the complex bottom topography (shallow in the TS and steep in the SCS) and a great influence on the wind-induced circulation (monsoon winds, local winds) making large variations on the distribution, propagation and dissipation of the tidal energy and currents (Zu et al., 2007; Doong et al., 2011). The mean tidal range in its north-western end is larger than 4 m while that in the south-eastern end is smaller than 1 m.

The East coast looks out onto the abyssal depths of the western North Pacific (WNP) and the Kuroshio surface current. The Kuroshio originates from the North Equatorial Current in the western Equatorial Pacific Ocean, fringes the Philippine islands and then diverts South of Taiwan between two branches making a loop South-West Taiwan in the South China Sea. The fastest northward directed branch is located East of Taiwan with currents reaching a depth of 1000 m at some latitudes. There, the mean Kuroshio velocity between 0 and 50m reachs up to 1.3 m/s at a distance between 20 and 40 km from the East coast (Hsin et al., 2008). The main branch then turn east after passing along Taiwan to follow the Okinawa Trough.

Climate

Taiwan is crossed by the Tropic of Cancer. This humid subtropical region experiences a Monsoon season from October to May, characterized by a constant medium northly wind and a typhoon season from June to August, characterized by a fair weather disrupted by strong energetic typhoons (Figure 2). The island is located on the most of typhoon's tracks which come from the western North Pacific (WNP). Every year, three or four typhoons strike Taiwan directly and around twenty pass near it bringing abundant rainfall to the area (Lin et al., 2009).

Hydrography and field site

The annual rainfall reaches 2500 mm, which is 2.5 times the world average. However, rainfall concentrates between May and October, with 75% of the total annual rainfall. Taiwan has 129 rivers, most of which are short with small and steep drainage basins with rapid flows. Due to the topography of the land, most rivers flow East or West. The runoff concentration time of the rivers is quite short. The longest river, the Choschui river, is only 186 km long, but its steepness is approximately 1/60. Because the rivers are short and steep, water discharges respond rapidly to rainfall intensity (Doong et al., 2011).

These conditions make Taiwan one of the most vulnerable area frequently suffering from nature disasters. The south-western coast of Taiwan displays a single well-expressed lagoonal system which is regularly exposed to extreme meteoroligical events. Ours study focuces on the Wan-Tzu-Liao sand barrier which pro-

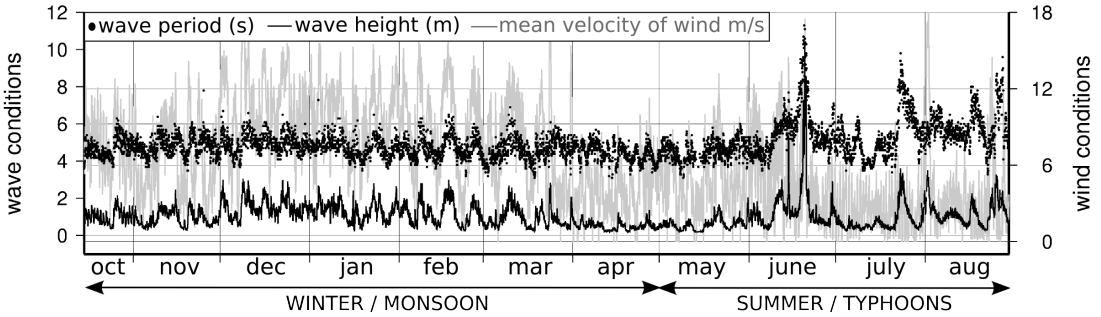

Figure 2: Wind/wave conditions at the CIGU buoy during the simulated period (Campmas et al., 2014).

tects the Cigu lagoon and harbour. The barrier of Wan-Tzu-Liao (Figure 1B) is a 7km long and 100-500m wide sand barrier, located on the Taiwan Strait near Tainan city.

NUMERICAL MODEL AND DRIVING FORCES

SYMPHONIE : 3D coastal circulation model

SYMPHONIE is an hydrostatic coastal circulation model developed by the SIROCCO team (Marsaleix et al., 2008) (Table 1). The components of the current, the temperature and the salinity are computed on a staggered C-grid thanks to a classic finite difference method. A generalized sigma coordinate (Ulses et al., 2008) is used in order to refine resolution near the bottom and the surface with special attention paid to the pressure gradients (Marsaleix et al., 2009, 2011). To this vertical grid is associated a polar curvilinear horizontal grid which refines the resolution near the coast while keeping reasonable computing times (Bentsen et al., 1999). We compute the baroclinic and barotropic velocity components separately following the time stepping method consisting of a Leap Frog scheme combined to a Laplacian filter (Marsaleix et al., 2012).

Table 1: Description of the SYMPHONIE model

Numerical method	C-grid, s coordinate, energy conserving	Marsaleix et al. (2008)
Time Stepping	Leap-Frog+Laplacian Filter	Marsaleix et al. (2012)
Pressure Gradient	Pressure Jacobian	Marsaleix et al. (2009)
Equation of state	McDougall 2003	Marsaleix et al. (2011)
Open boundary conditions	Radiation conditions	Marsaleix et al. (2006)
Sea surface conditions	Bulk formulae, Craig & Banner TKE boundary conditions	Estournel et al. (2009)
Turbulence closure	K-eps	Michaud et al. (2012)
Tides	Tide potential & TUGO nesting	Pairaud et al. (2008)
T,S advection	QUICK	
River input	Lateral condition	Estournel et al. (2001)
Wave effect	glm2z-RANS theory	Michaud et al. (2012)

Radiative conditions are applied at the lateral open boundaries (Marsaleix et al., 2006). The large scale forcing terms, included in the radiation conditions formulation, are provided by the daily outputs of the MERCATOR system (Madec, 2008). The relevant questions related to the nested models are discussed in Estournel et al. (2009) and Auclair et al. (2006). The high frequency barotropic forcing is provided by the FES2012 global tidal atlas (Lyard et al., 2006) and the astronomical tide potential has been implemented in the momentum equations according to Pairaud et al. (2008).

The air/sea fluxes are computed by the bulk formulae detailled in Estournel et al. (2009) and are provided by the ECMWF system (Dee et al., 2011). The river discharge is introduced through a lateral volume and salt conserving condition (Reffray et al., 2004).

The model domain

In this numerical simulation, we used a large scale domain ranging 600 km off the Taiwan island (Figure 3) in order to reduce the effect of erroneous boundary conditions and to reproduce as best as possible

remote effects of typhoons. The grid has 822 x 322 nodes, with a varying resolution from 5.6 km at the offshore to 460 m in the nearshore. This polar grid allows condensing the grid points in the area of interest, thus helping to avoid an excessive computational load. The vertical discretization is 40 sigma levels.

The GEBCO bathymetry data (8 min), a 100 m bathymetry resolution acquired during the ACT cruise in 1996 (Lallemand et al., 1997) and a high resolution bathymetry (10 m) made by the KUNSHEN project were combined to characterized the water depth on the computational grid.

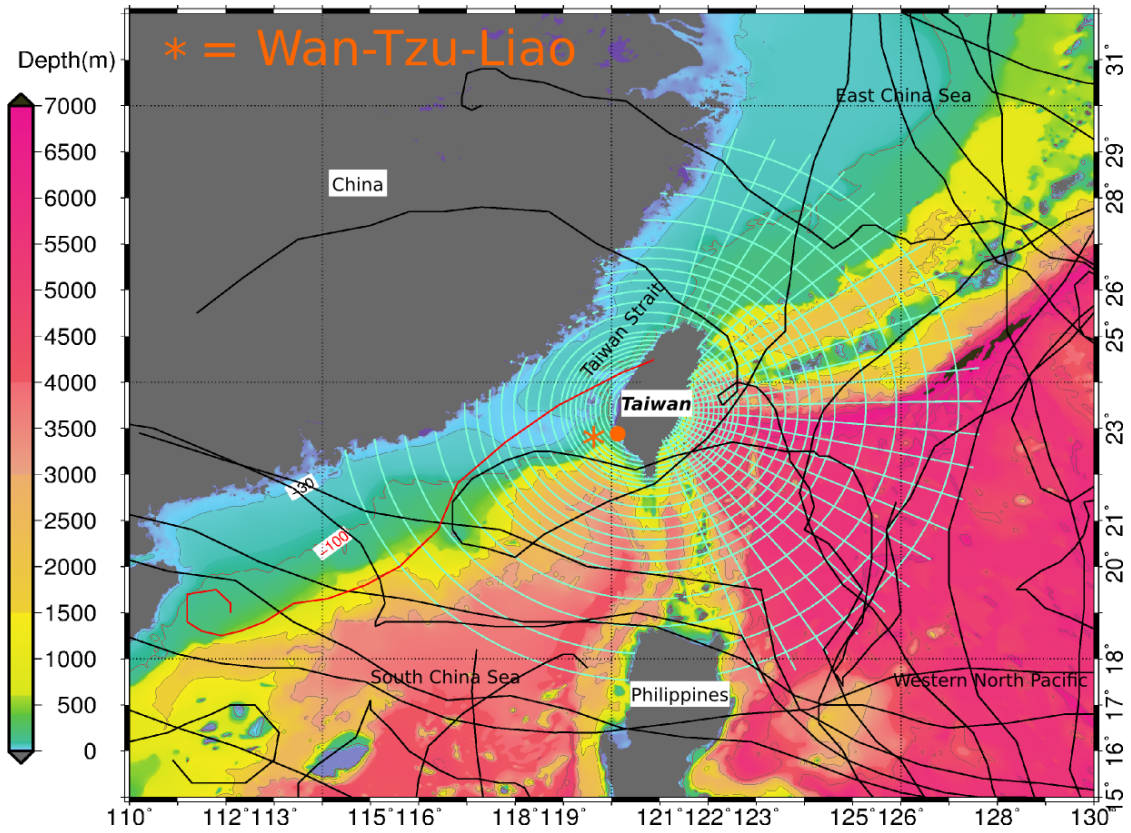

Figure 3: The regional polar grid with a nearshore resolution of 460 m in the nearshore and 5.6 km at the offshore and typhoon tracks during the simulation period. The red track is the TALIM typhoon.

The simulated period

Our simulation lasts from September 2011 to December 2012. This period includes the monitored period of the KUNSHEN project. The figure 3 shows the typhoons tracks recorded during this period. We have 17 typhoons which passed over the domain classified in tropical depressions or typhoons. Table 2 shows typhoon characteristics provided by the Japan Meteorological Agency (JMA) and the storm surge measured in the Chung-Chin harbour. The storm surge is given by : *Observed Water Level − Predicted Water Level.*

Table 2: Overview of the typhoons which passed over your domain during the simulated period.

Name	Time period (UTC)	Max wind velocity (m/s)	Min pressure (hPa)	Max storm surge (cm) *
NESAT	2011-09-23 - 2011-09-30	41.15	950	+29.2
NALGAE	2011-09-26 - 2011-10-05	48.87	935	+29
BANYAN	2011-10-09 - 2011-10-14	18	1002	+15.6
MAWAR	2012-05-31 - 2012-06-13	38.58	960	+9
GUCHOL	2012-06-10 - 2012-06-22	51.44	930	+22.7
TALIM	2012-06-16 - 2012-06-20	25.72	985	+23.6
DOKSURI	2012-06-25 - 2012-06-30	20.57	992	+3.7
KHANUN	2012-07-14 - 2012-07-20	25.72	985	+5.5
VICENTE	2012-07-18 - 2012-07-25	41.15	950	+18.2
SAOLA	2012-07-26 - 2012-08-05	36	960	+26.7
HAIKUI	2012-08-01 - 2012-08-11	33.43	965	-
KAI-TAK	2012-08-12 - 2012-08-18	33.43	970	+4.7
TEMBIN	2012-08-17 - 2012-09-01	41.15	950	+6.5
BOLAVEN	2012-08-19 - 2012-09-01	51.44	910	+6.5
JELAWAT	2012-09-20 - 2012-10-03	56.58	905	+17.6
GAEMI	2012-09-29 - 2012-10-07	25.72	990	-
BOPHA	2012-11-25 - 2012-12-09	51.44	930	+14.6

* Observed at the Chung-Chin tide gauge.
- HAIKUI appeared in the same time as SAOLA but according to its track, only SAOLA impacted our area.
- GAEMI appeared in the same time as JELAWAT but according to its track, only JELAWAT impacted our area.

The highest sustained wind velocity and the smallest eye pressure on our area was observed during the typhoon JELAWAT at the end of September 2012. Its track was far from the East coast so it only caused a storm surge of +17.6 cm at the Chung-Chin harbour.

Regarding storm surge, the typhoons NESAT and NALGAE caused the highest storm surge around 30 cm. HAIKUI typhoon appeared in the same time as SAOLA but according to its track, only the surge of SAOLA could be measured. In the same manner, only JELAWAT could be measured when GAEMI occured in the same time.

Instrumental devices

In the framework of the KUNSHEN project (ANR/NSC), a raft of devices were set in front of the Wan-Tzu Liao barrier (Figure 1B) during 7 months of monitoring including the simulated period. The equipments were deployed along a cross-shore section (in 18 m, 7 m, 4 m of water depth and on the emerged beach) and provided robust informations on nearshore hydrodynamics and water levels.

We got the tide gauge measurement and the predicted water level from the Central Weather Bureau (Taiwan) at the Chung-Ching harbour over all the simulated period.

The driving forces

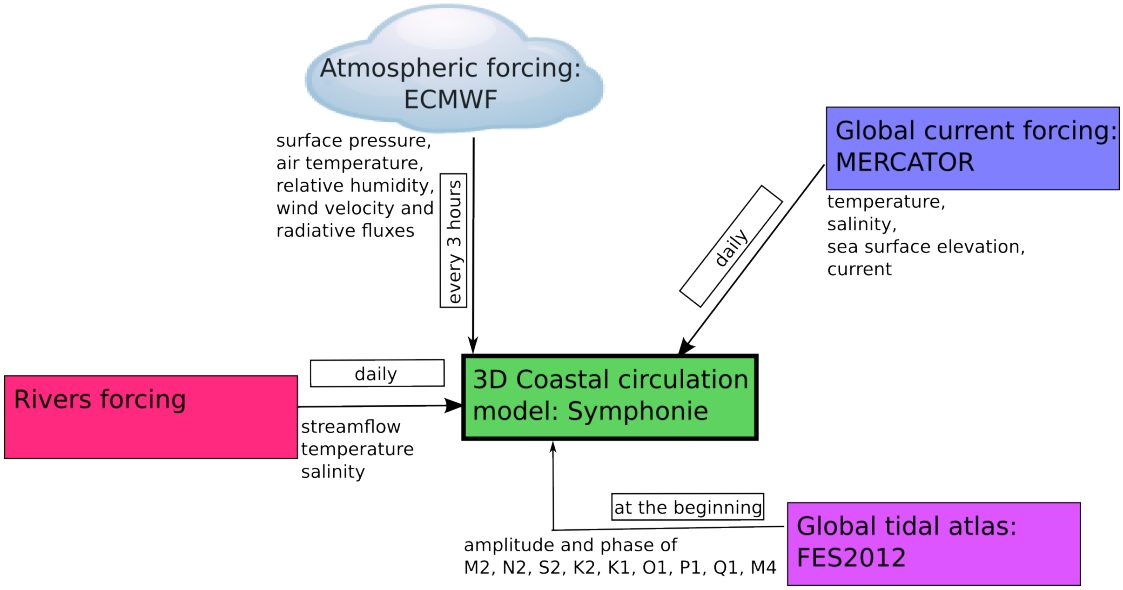

Figure 4: Overview of the SYMPHONIE's input forcings.

The simulation deals with most of the oceanographical forcings (winds, air/sea fluxes), global scale circulation (tides, Kuroshio current) and rivers (Figure 4). The variations of water level and currents at the boundaries are forced by the nine major diurnal and semidiurnal tidal constituents and a daily global oceanic circulation provided by the MERCATOR system (Madec, 2008). The four largest constituents along the Wan-Tzu-Liao barrier are associated with semidiurnal and diurnal effects of the moon and the sun (Table 3).

Table 3: Principal Tidal Constituents for ADCP 7m. This is the results of tidal decomposition made by T_tide (Pawlowicz et al., 2002) on data during July-August 2012.

Constituent	Amplitude (m)	Period	Description
M2	0.4649	12.42 h	Principal Lunar Semi-diurnal
K1	0.2085	23.93 h	Principal Lunar Diurnal
O1	0.1700	25.81 h	Principal Solar Dirunal
S2	0.1023	12 h	Principal Solar Semi-diurnal

Figure 5 shows the surface and bottom current provided by MERCATOR during the period. The surface current varied up to 88 cm/s and up to 53 cm/s for the bottom current. The intensity variation is more numerous during the typhoon season.

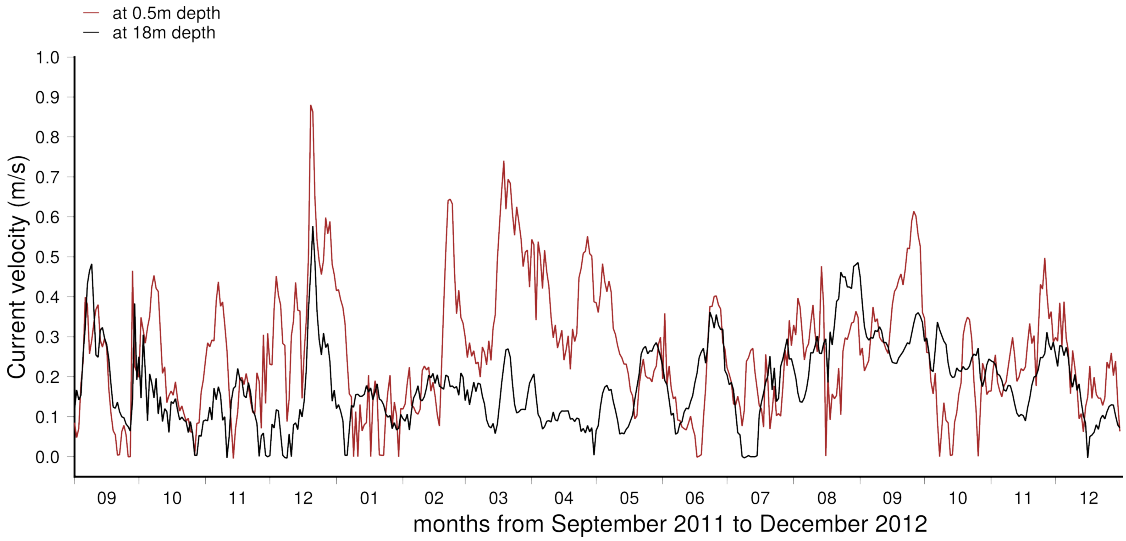

Figure 5: MERCATOR data of the surface and bottom current velocity at the CIGU buoy from September 1, 2011 to December 31, 2012.

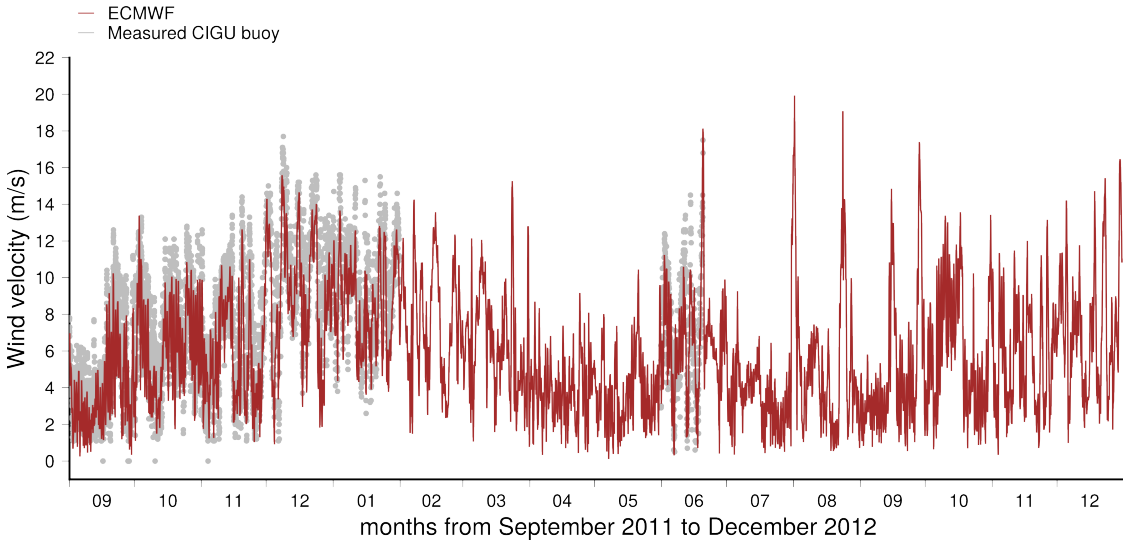

Figure 6: Comparison of wind velocity between ECMWF data and measurements at the CIGU buoy from September 1, 2011 to December 31, 2012.

The atmospheric conditions are provided every three hours by ECMWF (Era-Interim data ; Dee et al. (2011)) with a spacial resolution of 0.25 degres. According to this data (Figure 6), the wind velocity at the CIGU buoy varied up to 19.93 meters per second during the SAOLA typhoon. The river forcings are daily discharges of 21 rivers around Taiwan provided by the Ministry of Economic Affairs Water Resources Agency (Taiwan).

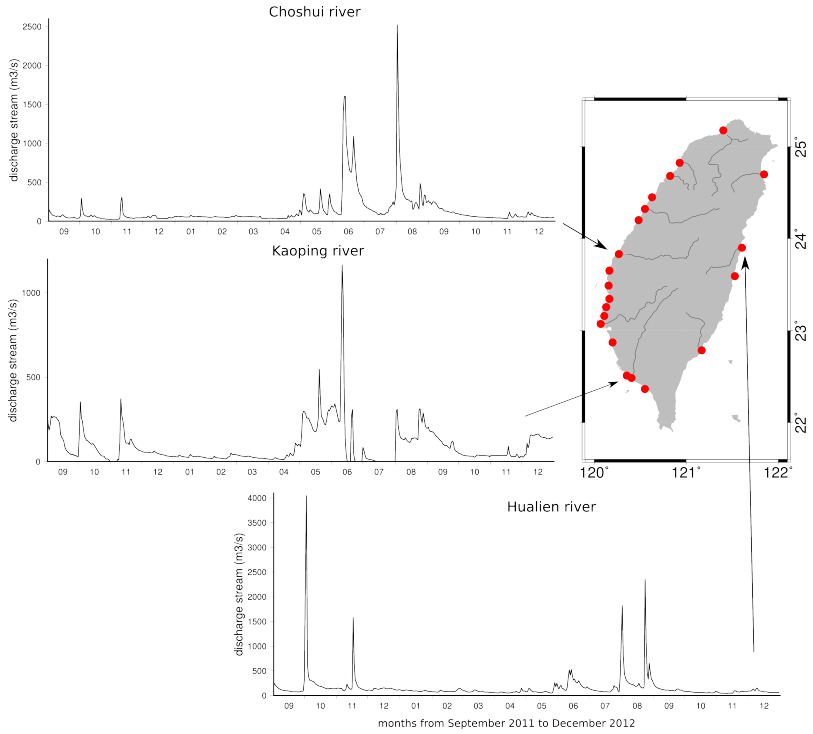

Figure 7: Location of the 21 rivers taken into account in the simulation and the stream flow of three main rivers during the considered period.

Figure 7 shows the location of the rivers around Taiwan and the behaviour of three main rivers : Choshui river, the longest one, Kaoping river located on the South-West coast and Hualien river on the East coast. Rivers are sensitive to the rainfall intensity and the water discharges can grow up to thousands cubic meters per second in few days.

RESULTS

To analyze the meteo-marine contributions, we ran our model forcing by forcing. For each typhoon event, we took the maximum sea surface height generated by the tide, the global currents and the atmospheric conditions at the Chung-Ching harbour.

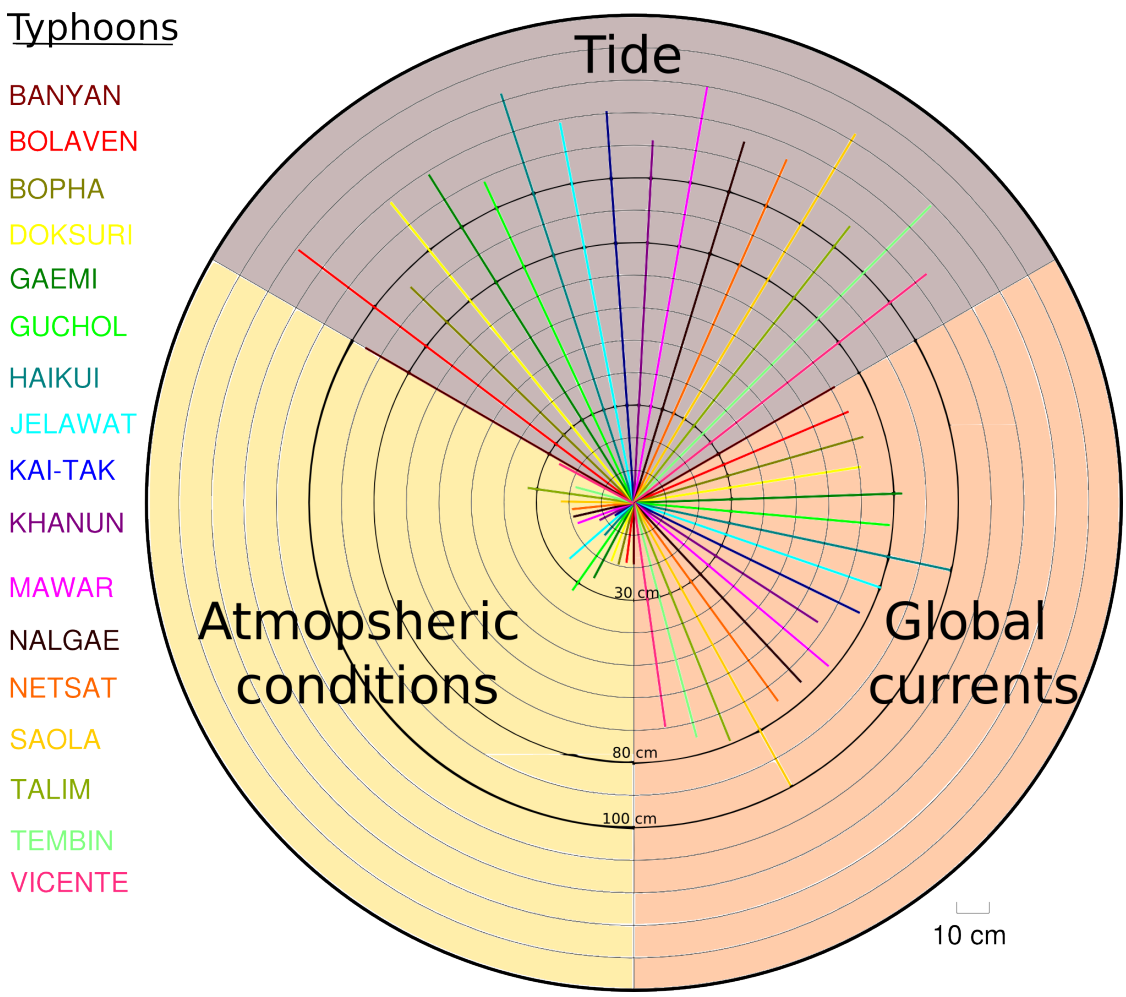

Figure 8: Contribution distribution between tide, global currents and atmospheric conditions at the Chung-Chin harbour during typhoon events. HAIKUI appeared in the same time as SAOLA but according to its track, only SAOLA impacted our area. GAEMI appeared in the same time as JELAWAT but according to its track, only SAOLA impacted our area.

Figure 8 shows that tide is the dominant forcing of the water level at the nearshore with more than 1 meter above the mean sea level. Global currents contribute up to 80 cm to the water level but during the SAOLA typhon, the elevation reached 1 meter. The contribution of atmospheric forcing is lower but it can generate 30 cm of elevation (e.g. during GUCHOL and TALIM typhoons).

DISCUSSION

Validation

In order to check the quality of our simulation, we compared the full-coupled simulation to measurements at the Chung-Chin harbour and at the ADCP 7m during the TALIM event (Figure 3).

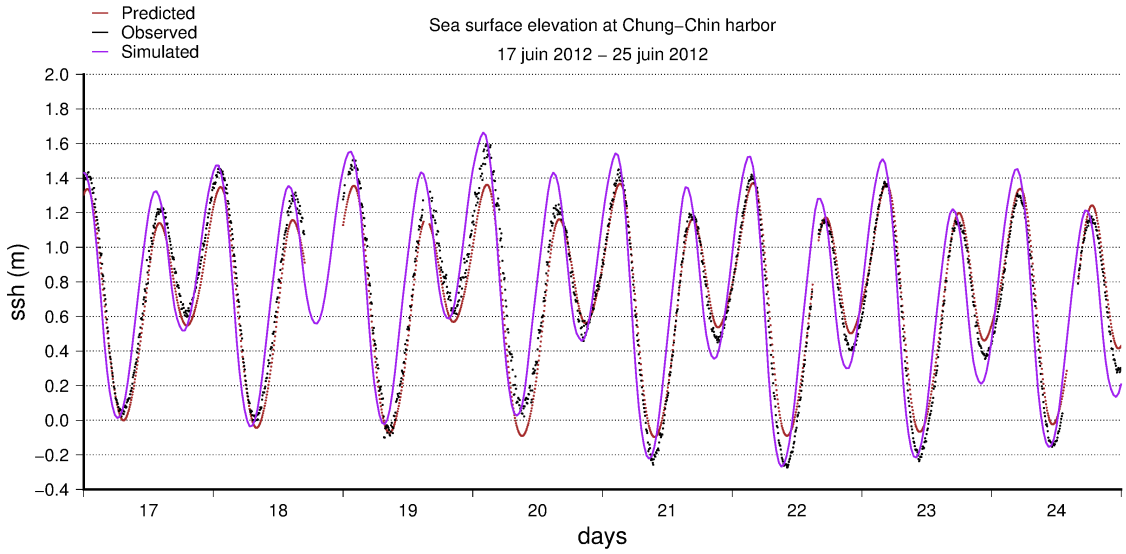

Figure 9: Comparison between the predicted/observed/simulated water level at the Chung-Chin harbour during the TALIM typhoon.

Results show that our model is in good agreement with the tide predictions and the observations. The storm surge on the 20th June is well reproduced. We can note that the model pre-empts the rising tide more especially during the storm. It also overestimates the days following the storm.

The wind forcing

We noted that the wind velocity from ECMWF and field measurement (Figure 6) show some discrepancies.

We quickly analyzed the signal by plotting a Quantile-Quantile plot (Figure 10) and it appeared that under 10 m/s, ECMWF underestimates the wind velocity and above 10 m/s it overestimates the velocity especially during the typhoon event.

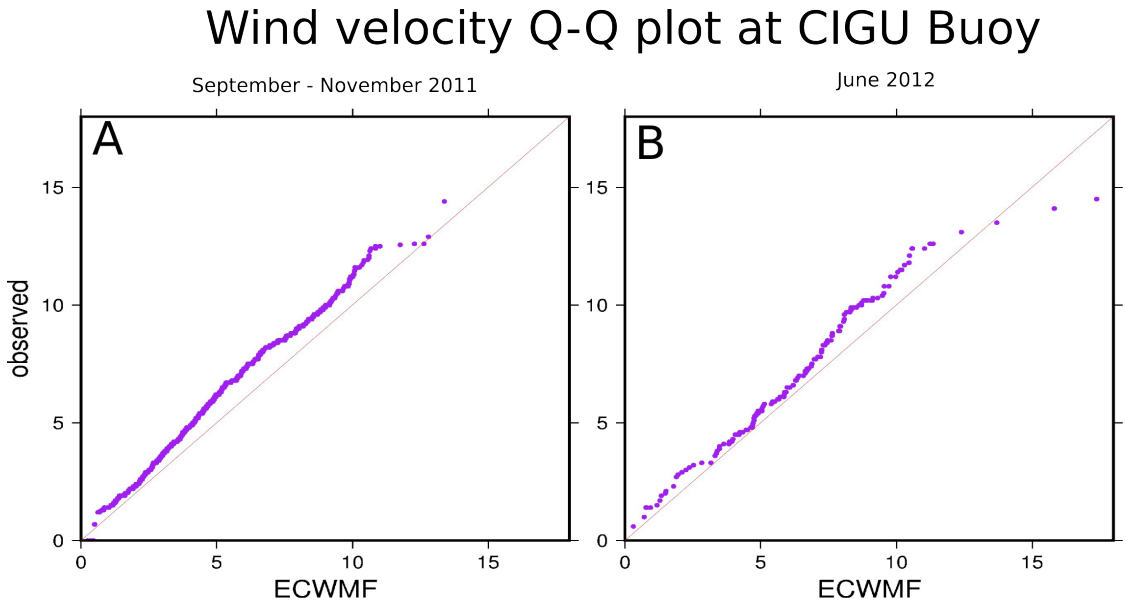

Figure 10: Quantile-Quantile plot of the wind velocity from ECMWF and measurement at the CIGU buoy. A) The period is September to November 2011; B) The period is June 2012.

Future works have to ensure that the representativeness of ECMWF's wind field could be a source of

bias.

The importance of the wave forcing

We perfomed a simulation without wave forcing. As shown by Michaud et al. (2012), the wave forcing during storm is very important to reproduce correctly the measurements at the nearshore. Future works have to compare the wave contribution against the others forcings.

Primitive equations & contribution analysis

This methodology contains some limitations by the fact that the momentum equations cannot separate totally the impacts of one forcing just by turning off the others. The atmospheric engine is an essential actor of the thermohaline circulation. By forcing our model only with the atmospheric conditions and a default initialization of the temperature (T) and salinity (S), we obtain an adjustment of sea surface height according to inert T & S fields.

CONCLUSIONS

We have analyzed the contributions of most of the oceanographical forcings to the exception of waves (atmospheric conditions, global scale circulation and rivers) during a contrasted range of meteo-marine conditions. Results show that tide is the dominant forcing of the water level at the nearshore, following by the global currents then atmospheric forcings. During GUCHOL and TALIM, atmospheric conditions generated 30 cm of elevation so it is important to not neglect this forcing when questions about the submersion are investigated.

ACKNOWLEDGEMENTS

We are grateful to GLADYS (http://www.gladys-littoral.org). Fabien Rétif was funded by the framework of the LITTOCMS project. We thank the HPC@LR center for running our model on their calculator.

References

F. Auclair, C. Estournel, P. Marsaleix, and I. Pairaud. On coastal ocean embedded modeling. *Geophysical Research Letters*, 33:L14602, 2006.

M. Bentsen, G. Evensen, H. Drange, and A. D. Jenkins. Coordinate transformation on a sphere using conformal mapping. *Monthly Weather Review*, 127:2733–2740, 1999.

A. J. Bowen, D. Inman, and V. P. Simmons. Wave 'set-down' and set-up. *Journal of Geophysical Research*, 73:2569–2577, 1968.

L. Campmas, F. Bouchette, S. Meulé, L. Petitjean, D. Sous, J.-Y. Liou, R. Leroux-Mallouf, F. Sabatier, and H.-H. Hwung. Typhoons driven morphodynamics of the wan-tzu-liao sand barrier (Taiwan). *Coastal Engineering 2014*, 1:1, 2014.

D. B. Chelton and D. B. Enfield. Ocean signals in tide gauge records. *Journal of Geophysical Research*, 91:9081–9098, 1986.

M.-D. Chiou, H. Chien, L. R. Centurioni, and C.-C. Kao. On the simulation of shallow water tides in the vicinity of the taiwan banks. *Terr. Atmos. Ocean. Sci.*, 21(1):45–69, 2010.

R. G. Dean and C. J. Bender. Static wave setup with emphasis on damping effects by vegetation and bottom friction. *Coastal Engineering*, 53:149–156, 2006.

D. Dee, S. Uppala, A. Simmons, P. Berrisford, P. Poli, S. Kobayashi, U. Andrae, M. Balmaseda, G. Balsamo, P. Bauer, P. Bechtold, A. Beljaars, L. van de Berg, J. Bidlot, N. Bormann, C. Delsol, R. Dragani, M. Fuentes, A. Geer, L. Haimberger, S. Healy, H. Hersbach, E. Holm, L. Isaksen, P. Kallberg, M. KÃ¶hler, M. Matricardi, A. McNally, B. Monge-Sanz, J.-J. Morcrette, B.-K. Park, C. Peubey, P. de Rosnay, C. Tavolatoe, J.-N. Thépaut, and F. Vitart. The ERA-Interim reanalysis: configuration and performance of the data assimilation system. *Quarterly Journal of the Royal Meteorological Society*, 137:553–597, 2011.

D.-J. Doong, H.-C. Chuang, C.-L. Shieh, and J.-H. Hu. Quantity, distribution, and impacts of coastal driftwood triggered by a typhoon. *Marine Pollution Bulletin*, 62:1446–1454, 2011.

C. Estournel, P. Broche, P. Marsaleix, J.-L. Devenon, F. Auclair, and R. Vehil. The rhone river plume in unsteady conditions: Numerical and experimental results. *Estuarine, Coastal and Shelf Science*, 53: 25–38, 2001.

C. Estournel, F. Auclair, M. Lux, C. Nguyen, and P. Marsaleix. âœscale orientedâ embedded modeling of the North-Western Mediterranean in the frame of MFSTEP. *Ocean Science*, 5:73–90, 2009.

Y.-C. Hsin, C.-R. Wu, and P.-T. Shaw. Spatial and temporal variations of the Kuroshio east of Taiwan, 1982–2005: A numerical study. *Journal of Geophysical Research*, 113:C04002, 2008.

S. Lallemand, C.-S. Liu, and the ACT scientific crew. Swath bathymetry reveals active arc-continent collision near taiwan. *American Geophysical Union*, 78:173–175, 1997.

G.-F. Lin, P.-Y. Huang, and G.-R. Chen. Using typhoon characteristics to improve the long lead-time flood forecasting of a small watershed. *Journal of Hydrology*, 380:450–459, 2009.

F. Lyard, F. Lefevre, T. Letellier, and O. Francis. Modelling the global ocean tides: modern insights from FES2004. *Ocean Dynamics*, 56:394–415, 2006.

G. Madec. *NEMO ocean engine*. Note du Pole de modélisation, Institut Pierre-Simon Laplace (IPSL), France, 2008. No 27 ISSN No 1288-1619.

P. Marsaleix, F. Auclair, and C. Estournel. Considerations on open boundary conditions for regional and coastal ocean models. *Journal of Atmospheric and Oceanic Technology*, 23:1604–1613, 2006.

P. Marsaleix, F. Auclair, J. W. Floor, M. J. Herrmann, C. Estournel, I. Pairaud, and C. Ulses. Energy conservation issues in sigma-coordinate free-surface ocean models. *Ocean Modelling*, 20:61–89, 2008.

P. Marsaleix, F. Auclair, and C. Estournel. Low-order pressure gradient schemes in sigma coordinate models: The seamount test revisited. *Ocean Modelling*, 30:169–177, 2009.

P. Marsaleix, F. Auclair, C. Estournel, C. Nguyen, and C. Ulses. An accurate implementation of the compressibility terms in the equation of state in a low order pressure gradient scheme for sigma coordinate ocean models. *Ocean Modelling*, 40:1–13, 2011.

P. Marsaleix, F. Auclair, T. Duhaut, C. Estournel, C. Nguyen, and C. Ulses. Alternatives to the Robert–Asselin filter. *Ocean Modelling*, 41:53–66, 2012.

H. Michaud, P. Marsaleix, Y. Leredde, C. Estournel, F. Bourrin, F. Lyard, C. Mayet, and F. Ardhuin. Three-dimensional modelling of wave-induced current from the surf zone to the inner shelf. *Ocean Science*, 8: 657–681, 2012.

I. Pairaud, F. Lyard, F. Auclair, T. Letellier, and P. Marsaleix. Dynamics of the semi-diurnal and quarter-diurnal internal tides in the Bay of Biscay. Part 1: Barotropic tides. *Continental Shelf Research*, 28: 1294–1315, 2008.

R. Pawlowicz, B. Beardsley, and S. Lentz. Classical tidal harmonic analysis including error estimates in matlab using t_tide. *Computers & Geosciences*, 28:929–937, 2002.

D. T. Pugh. *Tides, Surges and Mean Sea-Level*. John Wiley & Sons Ltd, Chichester, 1987.

G. Reffray, P. Fraunie, and P. Marsaleix. Secondary flows induced by wind forcing in the Rhône region of freshwater influence. *Ocean Dynamics*, 54:179–196, 2004.

C. Ulses, C. Estournel, P. Puig, X. D. de Madron, and P. Marsaleix. Dense shelf water cascading in the northwestern Mediterranean during the cold winter 2005: Quantification of the export through the Gulf of Lion and the Catalan margin. *Geophysical Research Letters*, 35:L7610, 2008.

D.-P. Wang and A. J. Elliott. Non-tidal variability in the chesapeake bay and potomac river: evidence for non-local forcing. *Journal of Physical Oceanography*, 8:225–232, 1978.

J. E. H. Weber, K. H. Christensen, and C. Denamiel. Wave-induced setup of the mean surface over a sloping beach. *Continental Shelf Research*, 29:1448–1453, 2009.

W. Zhang, F. Shi, H. Hong, S. Shang, and J. T. Kirby. Tide surge interaction intensified by the taiwan strait. *Journal of Geophysical Research*, 115:C06012, 2010.

T. Zu, J. Gan, and S. Y. Erofeeva. Numerical study of the tide and tidal dynamics in the South China Sea. *Deep-Sea Research*, 55:137–154, 2007.